Journal of Photochemistry and Photobiology A: Chemistry 222 (2011) 192–202

Contents lists available at ScienceDirect

Journal of Photochemistry and Photobiology A: Chemistry

journal homepage: www.elsevier.com/locate/jphotochem

Meta versus *para* substituent effect of organic dyes for sensitized solar cells

Yan-Duo Lin[a], Ching-Ting Chien[a], Szu-Yu Lin[a], Heng-Hsuan Chang[b], Ching-Yang Liu[b], Tahsin J. Chow[a,*]

[a] *Institute of Chemistry, Academia Sinica, Taipei 115, Taiwan*
[b] *Department of Applied Chemistry, Chinese Culture University, Taipei 111, Taiwan*

ARTICLE INFO

Article history:
Received 12 March 2011
Received in revised form 10 May 2011
Accepted 29 May 2011
Available online 21 June 2011

Keywords:
Dye-sensitized solar cell
Meta substituent effect
Stilbene
Charge transfer

ABSTRACT

A series of new metal-free organic donor-bridge-acceptor dyes comprising a triphenylamine moiety as the electron donor, and a cyanoacrylic acid (dye series A) or a carboxylic acid moiety (dye series B) as the electron acceptor were synthesized and utilized for dye-sensitized solar cells (DSSCs). The triphenylamine moiety was linked to the main chromophore through either a *para* or a *meta* position across a phenyl group in order to examine the difference of structural effect. Both types of compounds exhibited apparent solvatochromic shift in their fluorescence spectra, showing the ready formation of charge separated states in both the *para* and *meta*-isomers. Quantum mechanical calculations were performed by using the density functional theory (DFT) at the B3LYP/6-31G(d,p) level to gain insight into the electron distributions surrounding the *para* and *meta*-substituted triphenylamine groups. The movement of an electron from the donor to the acceptor under the irradiation of light can be depicted by the time-dependent DFT (TDDFT) calculations, and the results were compared with experimental observations. These dyes were used effectively as sensitizers in DSSCs after being absorbed on surface of nanocrystalline TiO_2. The incident photo-to-current conversion efficiency (IPCE) spectra of the *para* isomers are broader than that of the corresponding *meta* isomers, and the short-circuit current density (J_{sc}) values of the former is also higher than the latter. Dyes of series A exhibited overall conversion efficiencies of 1.27–4.12%, depending on the relative values of J_{sc}, under AM 1.5 G irradiation (100 mW cm^{-2}). For dyes of series B, the *para* isomers showed overall better performance than the *meta* isomers, i.e., higher values for all three parameters J_{sc}, V_{oc} (open-circuit voltage), and ff (fill factor), thus led to a higher conversion efficiency.

© 2011 Elsevier B.V. All rights reserved.

1. Introduction

The concern of global warming resulted from increasing energy consumption and environmental pollution has led to an intensive search for clean and renewable energy sources over the past decades. Dye-sensitized solar cells (DSSCs) have received considerable attention since the first report by O'Regan and Grätzel et al. in 1991 [1]. The Ru based sensitizers such as N3 [2], N719 [3], and black dye [4] exhibited impressive solar energy-to-electricity conversion efficiencies up to ~11%. The high performance can be ascribed not only to their broad metal-to-ligand charge transfer (MLCT) absorption bands but also to their long excited-state lifetime. In recent years, the interest in metal-free organic sensitizers is increasing as alternates for Ru complexes because of their high absorptivity, tunable spectral and electrochemical properties, environmental friendliness and low-cost. A variety of organic dyes such as coumarin [5–7], merocyanine [8,9], cyanine [10,11], indoline [12], triphenylamine [13–24], dithieno[3,2-*b*:2′,3′-d]thiophene [25], carbazole [26,27], fluorene [28], and spirobifluorene [29] etc. have been developed and found to be promising candidates for DSSCs.

Most organic dyes used in DSSCs posses a dipolar structure with an electron donor (D) and an electron acceptor (A) separated by a π-conjugated bridge (B). The D-B-A architecture can facilitate an efficient intramolecular charge transfer (ICT) upon irradiation by light. The electron donor is usually a derivative of triphenylamine (TPA) with strong electron-donating ability, while the three propeller-shaped aryl rings provide a steric hindrance to prevent it from undesired aggregation [30,31]. The electron acceptor group is usually a carboxylic acid with or without an electron-withdrawing substituent, which also functions as an anchoring group to attach onto the surface of TiO_2. The use of carboxylic acid [2–4] as an acceptor has been reported to yield modest to high performance in the cases of porphyrin [32], phthalocyanine derivatives [33], as well as some metal-free organic dyes [15,34]. The cyanoacrylic acid with an electron-deficient cyano substituent has displayed even more remarkable performances in most organic dyes. Compared with carboxylic acid, the cyanoacrylic acid is able to induce a more extended red shift in the absorption spectra,

* Corresponding author at: 128 Academia Road Sec. 2, Taipei 115, Taiwan. Tel.: +886 2 2789 8637; fax: +886 2 2788 4179.
E-mail address: tjchow@chem.sinica.edu.tw (T.J. Chow).

1010-6030/$ – see front matter © 2011 Elsevier B.V. All rights reserved.
doi:10.1016/j.jphotochem.2011.05.022

therefore can harvest a broader range of photons in the incident light.

In several earlier reports, a structural-dependent substituent effect in electron transfer processes has been noticed, particularly for the difference between *meta* and *para*-substituted phenyl groups in π-conjugated systems [35–42]. It is known that *meta*-linked chromophores show a weaker electronic coupling in the ground state than the *para* analogues [43–45], yet it seems to be more stabilized in the excited state. A typical example can be demonstrated in the derivatives of *trans*-aminostilbene [37–42]. The *trans*-stilbenes bearing either a *meta* or a *para*-amino substituent display a similar solvatochromic effect in their fluorescence spectra, revealing that species of high polarity were formed in both cases. However, the fluorescence lifetime of *meta*-substituted *trans*-stilbenes are longer than those of *para*-substituted isomers in about one order of magnitude. A longer lifetime indicates a slower rate of internal charge recombination, therefore it would be beneficial to the promotion of quantum efficiency of DSSCs. In view of such an advantage, the *meta*-substituted aminostilbenes may perform differently from those *para*-substituted isomers with analogous structures.

In this work, the *meta* versus *para* structural effect is addressed according to the performance of DSSCs through investigation of a series of sensitizer dyes with both *meta* and *para*-arranged TPAs as the electron donors. Two pairs of molecules are prepared as shown in Fig. 1, where the acceptor group is either a cyanoacrylic acid or a benzoic acid. The results are discussed with the aid of theoretical computations, which provided detailed electronic configurations by using density functional theory (DFT) and time-dependent DFT.

2. Materials and methods

2.1. Synthesis

The synthesis of *meta* and *para*-substituted compounds were outlined in Scheme 1. The synthesis of dyes **p1A** [22], **p2A** [17], **p2B** [46] and **m2B** [46] have been reported in the literatures. The synthesis of *meta*-conjugated dye **m2A** started from a protected 3-bromobenzadehyde **3** [47], which was coupled with diphenylamine through a palladium-catalyzed aromatic C–N bond formation. The ethylene glycol protecting group was removed by acidic hydrolysis to yield compound **4** [48]. Subsequent Knoevenagel condensation reaction with cyanoacetic acid in the presence of ammonium acetate afforded the dye **m2A**. The preparations of **m1A** proceeded through a similar sequence starting from **5** [49], which was obtained from **4** by methylenation of the aldehyde group via a Wittig reaction. Compound **5** was coupled with *p*-bromobenzldehyde by a Heck-type reaction to afford **6**. The cyanoacrylic acid group of **m1A** was formed by Knoevenagel reaction with cyanoacetic acid. Dyes **m1B** and **p1B** were prepared from diphenylamine and the corresponding *meta* or *para*-dibromobenzene by a palladium-catalyzed C–N bond formation reactions to form **7** [50] and **8** [46], respectively, followed by a coupling reaction with a 4-vinylbenzoic acid to afford the desired compounds.

2.2. Experimental

Solvents for syntheses were reagent grade or HPLC grade, for spectra measurements were all HPLC grade. Compounds purchased from commercial sources were used as received. Electronic absorption and emission spectroscopic investigation in solution was conducted using Jasco V-530 double beam spectrophotometer and Hitachi F-4500 fluorescence spectrophotometer, respectively. Fluorescence lifetimes were also measured at room temperature by use of a Edinburgh FLS920 spectrometer. The instrument response function was calibrated by a scatter solution using a gated hydrogen arc lamp. The goodness of the nonlinear least-squares fit was judged by the reduced χ^2 value (<1.2 in all cases), the randomness of the residuals, and the autocorrelation function.

2.3. General procedures for Heck reaction

A heterogeneous mixture of 0.28 ml of triethylamine, 1.00 ml of DMF, 1.05 mmol of styrene derivatives, 2 mol% of $Pd(OAc)_2/Pd_2(dba)_3$, 4 mol% of P(*o*-tolyl)$_3$, and 1.00 mmol of aryl bromide under argon were heated at 80 °C for 18 h. The solution was cooled and then 20 ml of CH_2Cl_2 was added. The insoluble residue was filtered off and the filtrate was concentrated *in vacuo* to afford a crude product. Further purification was performed by column chromatography.

2.4. General procedures for Knoevenagel condensation reaction

A mixture of aldehyde precursor (1.10 mmol), cyanoacetic acid (1.30 mmol), and ammonium acetate (0.28 mmol) in acetic acid (20 ml) was placed in a three-necked flask under nitrogen atmosphere and was stirred at 80 °C for 18 h. After cooling, the reaction was extracted with CH_2Cl_2. The organic layer was dried over anhydrous $MgSO_4$. The filtrate was concentrated under reduced pressure. Purification was performed by recrystallization in CH_2Cl_2/hexane.

2.5. Synthesis of 2-(m-bromophenyl)-1,3-dioxolane(*3*)

Ethylene glycol (40 g, 650 mmol) and *p*-toluenesulfonic acid monohydrate (0.16 g, 0.84 mmol) were added to a solution of *m*-bromobenzaldehyde (12 g, 65 mmol) in toluene (250 ml). The mixture was heated at reflux (130 °C) and by using a Dean–Stark apparatus to remove water. After stirred overnight, the mixture was cooled to room temperature and extracted with water/ethyl acetate. The organic layer was dried over anhydrous $MgSO_4$. The filtrate was concentrated under reduced pressure. Column chromatograph with ethyl acetate/hexane (1/20) afforded the desired product as colorless oil (14.30 g; 96% yield). ^{1}H NMR (400 MHz, $CDCl_3$): δ 7.66 (s, 1H), 7.51 (d, J = 7.6 Hz, 1H), 7.42 (d, J = 7.6 Hz, 1H), 7.26 (t, J = 7.8 Hz, 1H), 5.80 (s, 1H), 4.14–3.98 (m, 4H)ppm.

2.6. Synthesis of m-(diphenylamino)benzaldehyde(*4*)

Compound **3** (4.00 g, 17.5 mmol), diphenylamine (2.95 g, 17.50 mmol), $NaOBu^t$ (2.35 g, 24.50 mmol), DPPF (0.391 g, 0.70 mmol), and $Pd(OAc)_2$ (0.078 g, 0.35 mmol) in 40 ml of anhydrous toluene under nitrogen was heated at 80 °C for 18 h. The solution was cooled and then 20–30 ml of CH_2Cl_2 was added. The insoluble residue was filtered off and the filtrate was concentrated *in vacuo* to afford the crude product. Further purification was performed by column chromatography, using a mixed solvent ethyl acetate/hexane (1/20) as the elution to provide white solids in 72% yield. Mp 85–86 °C; ^{1}H NMR (400 MHz, $CDCl_3$): δ 7.28–7.22 (m, 6H), 7.15–7.09 (m, 6H), 7.07–7.01 (m, 2H), 5.71 (s, 1H), 4.14–3.96 (m, 4H) ppm. A mixture of this compound (4.00 g, 12.60 mmol), acetic acid (60 ml), THF (30 ml), and water (15 ml) was heated at 60 °C for 4 h. The reaction mixture was diluted with ethyl acetate, washed with water and saturated $NaHCO_3$. The organic layer was dried over anhydrous $MgSO_4$. The filtrate was concentrated under reduced pressure. Column chromatograph with ethyl acetate/hexane (1/20) afforded the desired product as yellow solid (1.13 g, 95% yield). Mp 90–91 °C; ^{1}H NMR (400 MHz,

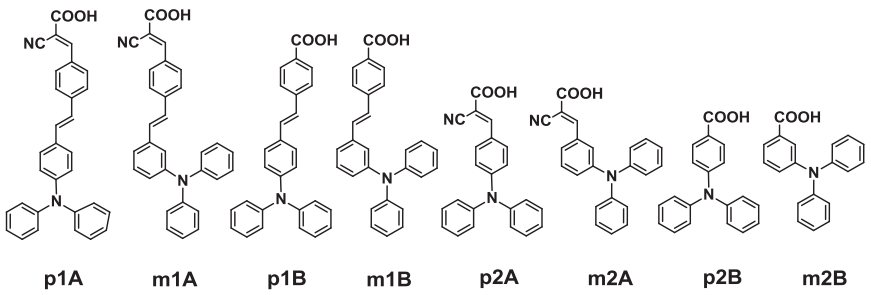

Fig. 1. Chemical Structures of the dyes.

$CDCl_3$): δ 9.88 (s, 1H), 7.54 (s, 1H), 7.47–7.45 (m, 1H), 7.38–7.26 (m, 6H), 7.11–7.05 (m, 6H) ppm.

2.7. Synthesis of m-(N,N-diphenylamino)styrene(**5**)

Methyltriphenylphosphonium iodide (2.28 g, 5.60 mmol) were dissolved in 25 ml of THF. NaH (0.31 g, 7.70 mmol) was added slowly in ice-water bath and then the mixture was stirring for another 2 h at ambient temperature. Compound **4** in THF (12 ml) was added dropwise to this reaction mixture by using a pressure-equalized addition funnel. After the completion of reaction, methanol was added at 0 °C to quench excess NaH and then the solvent was removed by rotary evaporation. Water was added to the reaction mixture, then it was extracted with ethyl acetate. The organic layer was combined and dried over anhydrous $MgSO_4$. The filtrate was concentrated under reduced pressure. Column chromatograph with ethyl acetate/hexane (1/20) afforded the desired product as a colorless liquid (9.23 g, 62% yield). ^{1}H NMR (400 MHz, $CDCl_3$): δ 7.26–7.18 (m, 5H), 7.13–7.08 (m, 6H), 7.03–6.96 (m, 3H), 6.61 (dd, J = 10.8, 18.6 Hz, 1H), 5.64 (d, J = 18.6 Hz, 1H), 5.19 (d, J = 10.8 Hz, 1H) ppm.

2.8. Synthesis of (E)-p-(m′-(diphenylamino)styryl)benzaldehyde (**6**)

Compound **6** was synthesized via the typical Heck reaction procedure as described above. Yellow solid was obtained in 25% yield. Mp 163–164 °C; ^{1}H NMR (400 MHz, $CDCl_3$): δ 9.98 (s, 1H), 7.84 (d, J = 7.8 Hz, 2H), 7.60 (d, J = 7.8 Hz, 2H), 7.59–7.19 (m, 7H), 7.13–7.11 (m, 5H), 7.11–7.01 (m, 4H); ^{13}C NMR (100 MHz, $CDCl_3$): δ 191.48, 148.41, 147.64, 143.30, 137.70, 135.32, 131.99, 130.14, 129.61, 129.29, 127.45, 126.86, 124.31, 124.11, 122.95, 122.41, 120.91 ppm. IR (KBr): 1690, 1568, 1274, 965, 692 cm^{-1}; FAB-HRMS calcd for $C_{26}H_{21}N_3$ (M^+) 365.1623, found 365.1616.

2.9. Synthesis of m-bromo-N,N-diphenylamine (**7**)

Compound **7** was synthesized according to the same procedure as that of **4**, giving **7** in 60% as white solid. Mp 95–96 °C; ^{1}H NMR

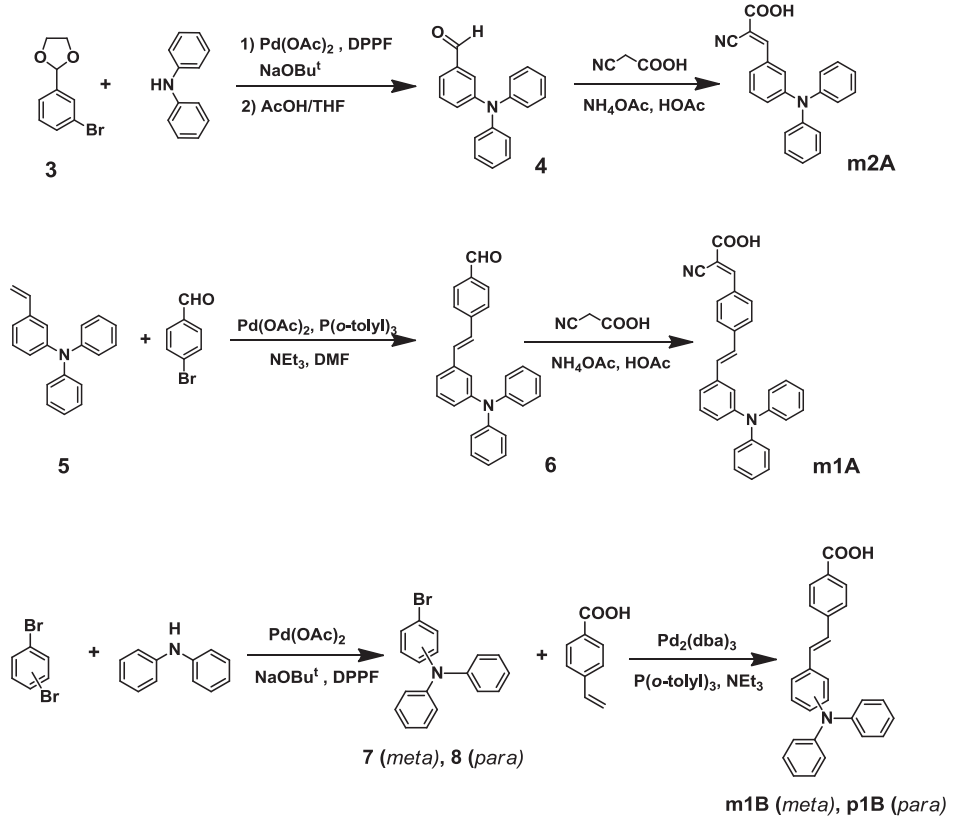

Scheme 1. Synthesis of the *meta* and *para*-substituted dyes.

(400 MHz, $CDCl_3$): δ 7.30–7.26 (m, 4H), 7.20 (s, 1H), 7.20–7.05 (m, 8H), 6.98–6.96 (m, 1H) ppm.

2.10. Synthesis of p-bromo-N,N-diphenylamine (**8**)

Compound **8** was synthesized according to the same procedure as that of **7**, giving **8** in 45% as white solid. Mp 113–114 °C; ^{1}H NMR (400 MHz, $CDCl_3$): δ 7.32 (t, *J* = 8.8 Hz, 2H), 7.29–7.20 (m, 4H), 7.05 (t, *J* = 7.8 Hz, 4H), 7.02–6.96 (m, 2H), 6.93–6.90 (m, 2H) ppm.

2.11. Synthesis of 2-cyano-3-(m-(diphenylamino)phenyl)acrylic acid (**m2A**)

Compound **m2A** was obtained according to the standard Knoevenagel condensation reaction as described above. Red solid of **m2A** was afforded in 65%. Mp 206–207 °C; ^{1}H NMR (400 MHz, $CDCl_3$): δ 8.29 (s, 1H), 7.87 (d, *J* = 7.6 Hz, 1H), 7.61 (s, 1H), 7.51–7.40 (m, 6H), 7.26–7.21 (m, 6H) ppm; ^{13}C NMR (100 MHz, $CDCl_3$): δ 156.83, 148.98, 146.90, 132.25, 130.12, 129.65, 127.53, 126.59, 125.50, 124.99, 123.99, 123.42, 114.69,100.19 ppm. IR (KBr): 2825, 2227, 1688, 1272 cm^{-1}; FAB-HRMS calcd for $C_{22}H_{16}N_2O_2$ (M^+) 340.1212, found 340.1214.

2.12. Synthesis of (E)-3-(p-((E)-m′-(diphenylamino)styryl)phenyl)-2-cyanoacrylic acid (**m1A**)

Compound **m1A** was obtained according to the typical Knoevenagel condensation reaction as described above. Red solid of **m1A** was afforded in 65%. Mp 257–258 °C; ^{1}H NMR (400 MHz, $CDCl_3$): δ 8.25 (s, 1H), 7.99 (d, *J* = 7.8 Hz, 2H), 7.56 (d, *J* = 8.0 Hz, 2H), 7.29–7.18 (m, 7H), 7.11–7.06 (m, 5H), 7.13–6.98 (m, 4H), ppm; ^{13}C NMR (100 MHz, $CDCl_3$): δ 157.02, 148.21, 146.36, 145.45, 143.06, 138.84, 137.32, 134.40, 127.40, 126.56, 125.98, 125.66, 124.58, 123.60, 120.84, 117.24, 114.57, 51.19, 38.96 ppm. IR (KBr): 2808, 1932, 1679, 1283, 956, 693 cm^{-1}; FAB-HRMS calcd for $C_{30}H_{22}N_2O_2$ (M^+) 442.1681, found 442.1679.

2.13. Synthesis of (E)-p-(m′-(diphenylamino)styryl)benzoic acid (**m1B**)

Compound **m1B** was synthesized via the standard Heck reaction procedure as described above, giving **m1B** as a light green solid in 27%. Mp 265–266 °C; ^{1}H NMR (400 MHz, $CDCl_3$): δ 8.05 (s, 1H), 7.99 (d, *J* = 8.2 Hz, 2H), 7.53 (d, *J* = 8.2 Hz, 2H), 7.28–7.18 (m, 8H), 7.14–7.10 (m, 4H), 7.04–6.96 (m, 4H) ppm; ^{13}C NMR (100 MHz, $CDCl_3$): δ 170.97, 148.42, 147.71, 142.63, 137.86, 131.53, 130.65, 129.62, 129.32, 127.89, 127.62, 126.41, 124.33, 124.06, 122.95, 122.47, 120.95 ppm. IR (KBr): 3025, 1686, 1588, 956, 696 cm^{-1}; FAB-HRMS calcd for $C_{27}H_{22}NO_2$ (M+H$^+$) 392.1651, found 392.1654. Anal. Calcd for $C_{27}H_{21}NO_2$: C, 82.84, H, 5.41, N, 3.58. Found: C, 82.94, H, 5.41, N, 3.50.

2.14. Synthesis of (E)-p-(p′-(diphenylamino)styryl)benzoic acid (**p1B**)

Compound **p1B** was synthesized according to the standard Heck reaction procedure as described above. Light green solid of **p1B** was afforded in 31%. Mp 247–248 °C; ^{1}H NMR (400 MHz, $CDCl_3$): δ 8.14 (s, *J* = 8.1 Hz, 2H), 7.61 (d, *J* = 8.1 Hz, 2H), 7.45 (d, *J* = 8.4 Hz, 2H), 7.34–7.26 (m, 4H), 7.22–7.04 (m, 10H) ppm; ^{13}C NMR (100 MHz, $CDCl_3$): δ 171.58, 148.08, 147.36, 143.10, 131.21, 130.66, 130.51, 129.32, 127.74, 127.53,126.10, 125.56, 124.75, 123.32,123.06, 122.95 ppm. IR (KBr): 3027, 1680, 1588, 957, 694 cm^{-1}; FAB-HRMS calcd for $C_{27}H_{22}NO_2$ (M+H$^+$) 392.1651, found 392.1652.

2.15. Computation methods

The computations were performed with the Gaussian 03 program package [51]. The geometry was optimized by using B3LYP (Becke three parameters hybrid functional with Lee-Yang-Parr correlation functionals) with the Pople 6-31G(d,p) atomic basis set [52,53]. The excitation transition of dyes were calculated using time-dependent density functional theory (TDDFT) calculations with B3LYP/6-31G(d,p).

2.16. Device fabrication

A thin film of TiO_2 (16–18 μm thick) was coated on a 0.25 cm^2 FTO glass substrate. It was immersed in a THF solution containing 3×10^{-4} M dye sensitizers for 12 h, then rinsed with anhydrous acetonitrile and dried. The relative loading amount depends on the nature of each compound, e.g. the quantity absorbed by **p1A** was higher than that of **m1A** (Table T1). Another piece of FTO with sputtering 100 nm thick Pt was used as a counter electrode. The active area was controlled at a dimension of 0.25 cm^2 by adhering 60 μm thick polyester tape on the Pt electrode. The photocathode was placed on top of the counter electrode and was tightly clipped together to form a cell. Electrolyte was then injected into the seam between two electrodes. An acetonitrile solution containing LiI (0.5 M), I_2 (0.05 M), and 4-*tert*-butylpyridine (0.5 M) was used as the electrolyte. Devices made of a commercial dye N719 under the same condition was compared as a reference. The cell parameters were obtained under an incident light with intensity 100 mW cm^{-2}, which was generated by a 300 W Xe lamp passing through an AM 1.5 filter. The current–voltage parameters of DSSCs were recorded by a potentiostat/galvanostat model CHI650B (CH Instruments, USA).

3. Results and discussion

3.1. Absorption spectra

The absorption spectra of dyes **A** and **B** in THF can be depicted in Fig. 2 and the data are listed in Table 1. All dyes displayed a strong absorption band at around 300 nm that was attributed to the π–π* transition. The lower energy bands at 350–450 nm with variable intensities, e.g. more intensive for *para*-conjugated dyes yet substantially weaker for *meta*-conjugated dyes, are assign to intramolecular charge transfer (ICT) transitions from the triarylamine donors to the carboxylic acid acceptors. This absorption spectra exhibited mild but negative solvatochromic shifts in more polar solvents. The phenomenon may be ascribed to the deprotonation of the carboxylic group, which weakens the electron-withdrawing ability of the acceptor (Figures. S2 and S3) [29]. For *meta*-linked dyes, the low-intensity ICT bands are attributed to a lower degree of electronic coupling between the donor and acceptor [37–42]. Comparing the dyes with the same backbone but different geometry of the donor groups, the absorption bands of *para*-conjugated dyes were more red-shifted when compared with the corresponding *meta*-conjugated dyes, as a result of better resonance in the former. For example, the ICT band of **p1A** (λ_{max} at 433 nm) is substantially red-shifted in comparison with that of **m1A** (367 nm). It is also noteworthy that for *meta*-linked isomers, particularly for **m1A**, the electron migration is likely to have proceeded from the central stilbene moiety, instead of TPA, to the terminal acceptor group (Figures S4 and S5). To compare the absorption spectra between the dyes in series **A** and **B**, the spectra of dyes in **A** extended to longer wavelength regions than those in series **B** due to a longer chromophores introduced by the cyanoacrylate group. The molar extinction coefficients of

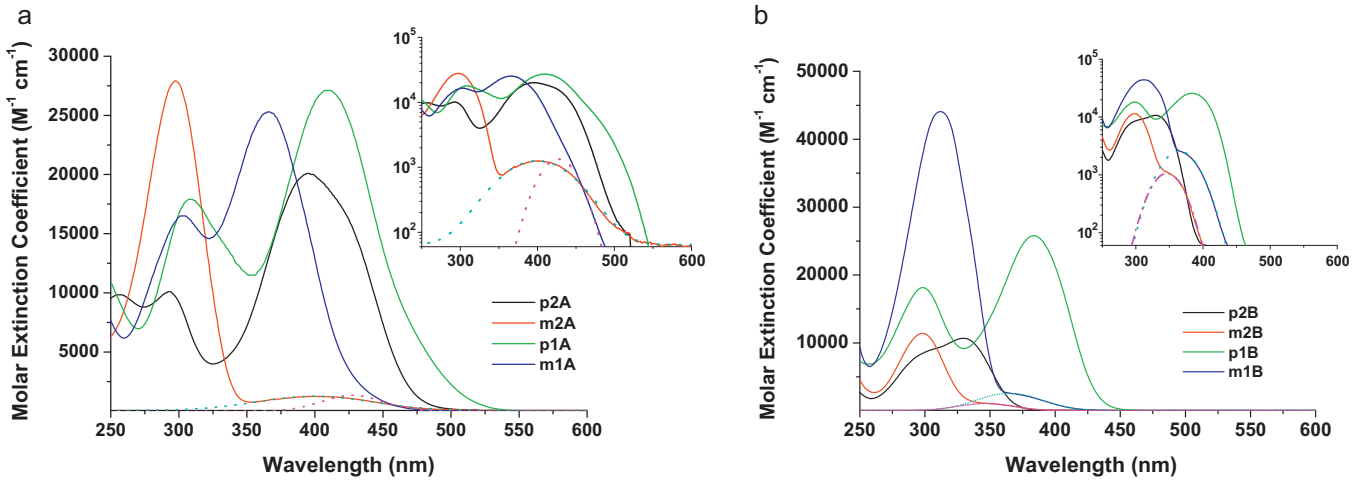

Fig. 2. Absorption spectra of (a) dye **A** and (b) dye **B** in THF solutions. Gaussian deconvolutions of the longest wavelength transitions in the absorption spectra of **m1A**, **m2A**, **m1B** and **m2B** are shown as dotted lines. Figures in the insets are expressed in logarithm scale in order to illustrate the weaker absorption bands.

dyes **A** range in 20,100–27,900 M^{-1} cm^{-1}, and those of dyes **B** in 10,100–44,100 M^{-1} cm^{-1}, while both are larger than that of N719 (14,100 M^{-1} cm^{-1}) except **p2B** and **m2B**, revealing that these dyes are suitable for harvesting light in high efficiency.

Spectral deconvolution with Gaussian curves allows us to estimate the peak maxima of *meta* isomers as well as the oscillator strengths (f) of the $S_0 \rightarrow S_1$ transitions. These data are presented in Table 1. The oscillator strengths of the ICT transitions for *meta*-substituted derivatives are found to be significantly weaker than those for the corresponding *para* isomers. Within the same series of *para* linked structures, the dyes with cyanoacrylic acid anchoring group (series **A**) exhibited larger f values than the corresponding carboxylic ones (series **B**), e.g., the comparison between **p1A** and **p1B**. Both observations are well consistent with the computational results of TDDFT shown in the following.

3.2. Fluorescence spectra

Fluorescence spectra of dyes in series **1** are shown in Fig. 3. All emission displayed apparent red shifts in more polar solvents, indicating a strong ICT character in the excited state. It was unusual, however, to have observed a significant blue shift for compound **p1A** in acetonitrile. The reason can be ascribed to deprotonation, the same phenomenon as what observed in the absorption spectra, which considerably lowered the potential energy of the ground state. Cyanoacrylic acid terminated dyes display more red-shifted than the corresponding benzoic acid ones due to a longer length of π-chromophores. It should be noted that the magnitude of bathochromic shift for *meta* derivatives are similar to those for the corresponding *para* isomers, e.g., **p1A** vs **m1A**, and **p2B** vs **m2B**, indicating that the dipole moment of both isomers are similar in the excited state. Such phenomena have been reported previously in *meta* and *para* donor–acceptor-substituted benzenes [54]. The fluorescence maxima (λ_f) and the Stokes shift ($\Delta\nu_{st}$), measured by the gap between absorption and fluorescence spectra, and of dyes **A** and **B** are summarized in Table 1.

The charge transfer nature of the excited state can be verified by examining the polarity of the compounds. The dipole moment of excited state can be estimated from the amount of Stokes shift against the solvent parameter Δf according to Eq. (1) [55]

$$\nu_f = -\left[\left(\frac{1}{4\pi\varepsilon_0}\right)\left(\frac{2}{hca^3}\right)\right][\mu_e(\mu_e - \mu_g)]\,\Delta f + \text{constant} \quad (1)$$

where

$$\Delta f = \frac{(\varepsilon - 1)}{(2\varepsilon + 1)} - \frac{0.5(n^2 - 1)}{(2n^2 + 1)} \quad (2)$$

and

$$a = \left(\frac{3M}{4N\pi d}\right)^{1/3} \quad (3)$$

where ν_f is the fluorescence maxima; a is the solvent cavity (Onsager) radius, calculated from the Avogadro number (N), molecular weight (M), and density (d) according to Eq. (3); ε, ε_0, and n are solvent dielectric constant, vacuum permittivity, and solvent

Table 1
Maxima of UV absorption (λ_{abs}) and fluorescence (λ_f), fluorescence decay times (τ_f), 0-0 transition ($\lambda_{0,0}$), Stokes shifts ($\Delta\nu_{st}$), oscillator strength (f) for $S_0 \rightarrow S_1$ band of dyes **A** and **B** in tetrahydrofuran (THF).

Compd	λ_{abs} (nm)[a]	λ_{max} ($\varepsilon \times 10^{-4}$, dm^3 mol^{-1} cm^{-1})	τ_f (ns)[b] (preexp%)	λ_f (nm)	λ_{0-0} (nm)[c]	$\Delta\nu_{st}$ (cm^{-1})[d]	f[e]
m1A	303, 367 (427)	2.53	4.16 (8), 16.76 (92)	519	455	4150	0.02
p1A	310, 433	2.71	2.29	607	482	6620	0.66
m2A	298 (400)	2.79	nd[f]	504	458	5160	0.04
p2A	293, 395	2.01	nd[f]	537	447	6690	0.49
m1B	313, (365)	4.41	1.58 (5), 17.38 (95)	489	410	6950	0.05
p1B	298, 385	2.58	2.17	478	424	5050	0.47
m2B	298 (346)	1.01	nd[f]	442	391	6280	0.02
p2B	308, 329	1.07	nd[f]	425	373	6870	0.19

[a] The long wavelength weak absorption bands are in parentheses.
[b] Lifetime of emission bands excited at the major long wavelength absorption maxima.
[c] Obtained from the intersection of normalized absorption and fluorescence spectra.
[d] $\Delta\nu_{st} = \nu_{abs}$ ($S_0 \rightarrow S_1$) $- \nu_f$.
[e] $f = 4.3 \times 10^{-9}$ (ν) $d\nu$.
[f] Not determined.

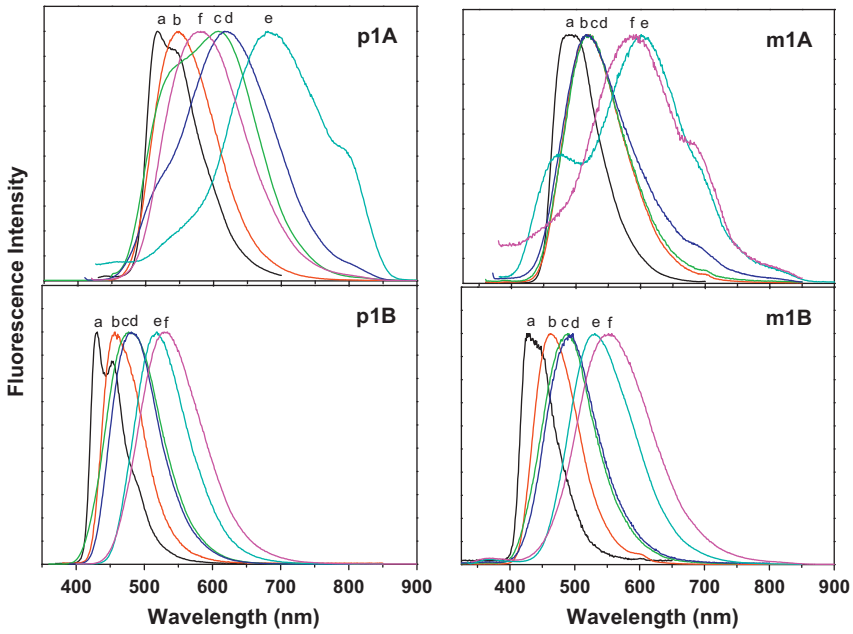

Fig. 3. Normalized fluorescence spectra of series **1** in (a) cyclohexane, (b) toluene, (c) THF, (d) ethyl acetate, (e) dichloromethane, and (f) acetonitrile.

refractive index, respectively. The value of μ_g was calculated using the DFT algorithm. The calculated dipole moments for dyes **A** and **B** and the slope (m_f) of the plots are listed in Table 2. The dipole moments of all compounds after the photo-excitation were significantly increased, e.g. 9–20 D vs. 2–9 D, as the result of ICT. In the typical example of **p1A**, the estimated difference was 10.7 D. The μ_e values of *para*-isomers are found to be larger than the corresponding *meta*-isomers in both the ground and excited states. This trend is reasonable considering the distance between D and A is longer in the former. The dipole moments of dyes **A** were larger than those of dyes **B**, i.e., 11–20 D vs. 9–16 D, as depicted by the wider spread of spectral shifts shown in Fig. 3 (top vs. bottom). It is likely due to a greater charge withdrawing ability of cyanoacrylic acid with respect to the benzoic acid.

The large μ_e values of both *meta* and *para*-isomers reveal clearly the presence of an ICT state at the lowest potential energy. The electronic configuration of ICT is further confirmed by TDDFT calculations as indicated below.

3.3. Fluorescence lifetimes

In the process of electron flow, the rate of electron injection from the dye to TiO_2 competes with the decay of charge-separated excited state. For typical Ru-complex dyes, the lifetime of excited state is relatively long, e.g., 20–60 ns [56]. A long excited state lifetimes, as mentioned in the preceding session, is beneficial to the quantum efficiency of DSSCs.

The phenomenon of a slower decay (>8 ns) for *meta*-substituted *trans*-3-aminostilbene have been well addressed in the literatures [37–42]. The room-temperature fluorescence lifetimes (τ_f) of **p1A**, **m1A**, and **p1B**, **m1B** in THF are measured and compared in Table 1. The lifetimes of *meta*-substituted dyes, i.e., **m1A** and **m1B**, are found to be about one order of magnitude longer than the corresponding *para* ones, i.e., **p1A** and **p1B**. However, a double exponential function is necessary to fully describe the decay curves of **m1A** and **m1B**. The dual exponential decay can be attributed to the coexistence of different conformers in the solution [39]. The longer lifetime of *meta*-substituted dyes is expected to be favorable to the performance of DSSC.

3.4. Molecular orbital calculation

The photophysical nature of both series **A** and **B** compounds, i.e. the spectroscopic properties and the solvatochromic shifts, may be rationalized more thoroughly with the aid of computations. The molecular orbitals of dyes **A** and **B** were performed by density functional theory (DFT) calculations [51] at B3LYP/6-31G(d,p) level with full geometry optimization [52,53]. The excited states were computed by time-dependent DFT (TDDFT) with B3LYP functional to compare with the experimental results. The electron distributions of the HOMO, HOMO-1 and LUMO of the dyes are shown in

Table 2
Ground and excited-state dipole moments.

Dye	A (Å)[a]	m_f (cm^{-1})[b]	μ_g (D)[c]	μ_e (D)
m1A	5.60	10,840	7.49	15.6
p1A	5.60	17,220	9.28	20.0
m2A	4.79	10,350	5.26	10.7
p2A	4.79	11,900	8.10	15.2
m1B	5.21	14,250	2.76	15.6
p1B	5.21	11,530	4.07	14.9
m2B	4.45	75,60	1.74	9.1
p2B	4.45	12,240	3.22	12.1

[a] Onsager radius from Eq. (3) with d = 1.0 for **m1A** and **p1A**, 1.1 for **m2A**, **p2A**, **m1B**, and **p1B**, and 1.3 g/cm^3 for **m2B** and **p2B**.
[b] Calculated based on Eq. (1).
[c] Calculated by use of DFT.

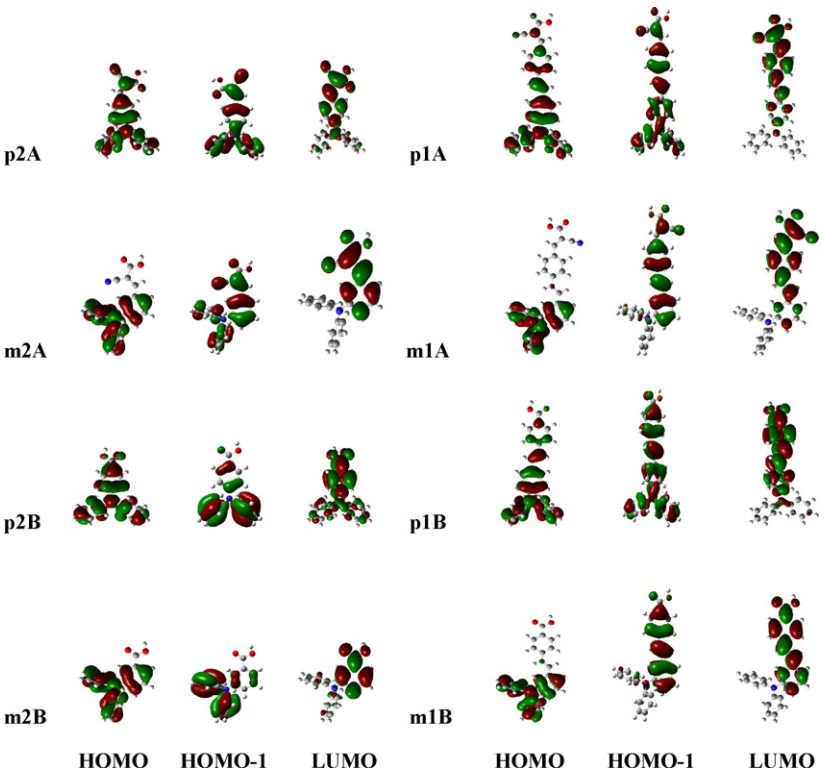

Fig. 4. Frontier orbitals of the dyes optimized with DFT at the B3LYP/6-31G(d,p) level.

Table 3
Calculated TDDFT excitation energies (*E*), oscillator strengths (*f*), MO compositions and characters, are compared with experimental absorptions.

Dye	n^a	*E* (ev, nm)	*f*	Composition	Character	Exptl (ev, nm)
m1A	1	2.18 (570)	0.03	98% HOMO → LUMO	CT	2.90 (427)
	2	3.04 (408)	1.33	95% HOMO-1 → LUMO	π–π* (1)	3.38 (367)
	5	3.94 (315)	0.18	69% HOMO-3 → LUMO	π–π* (2)	4.09 (303)
	7	4.07 (305)	0.10	71% HOMO → LUMO + 2	π–π* (3)	
	8	4.10 (303)	0.13	39% HOMO-4 → LUMO	π–π* (4)	
	10	4.14 (299)	0.22	81% HOMO → LUMO + 5	π–π* (5)	
p1A	1	2.32 (534)	0.95	98% HOMO → LUMO	CT	2.86 (433)
	2	3.31 (375)	0.98	82% HOMO-1 → LUMO	π–π* (1)	4.00 (310)
	5	4.01 (309)	0.13	88% HOMO → LUMO + 3	π–π* (2)	
m2A	1	2.23 (555)	0.01	98% HOMO → LUMO	CT	3.10 (400)
	3	3.92 (317)	0.19	62% HOMO-1 → LUMO	π–π* (1)	4.16 (298)
	4	3.98 (311)	0.38	80% HOMO→LUMO + 1	π–π* (2)	
	6	4.18 (297)	0.14	47% HOMO → LUMO + 3	π–π* (3)	
	9	4.25 (292)	0.13	41% HOMO → LUMO + 2	π–π* (4)	
	10	4.30 (288)	0.25	26% HOMO-5 → LUMO	π–π* (5)	
p2A	1	2.97 (417)	0.80	96% HOMO → LUMO	CT	3.14 (395)
	3	4.17 (298)	0.13	64% HOMO → LUMO + 1	π–π* (1)	4.23 (293)
	4	4.20 (295)	0.19	70% HOMO-1 → LUMO	π–π* (2)	
m1B	1	2.74 (452)	0.02	97% HOMO → LUMO	CT	3.40 (365)
	2	3.66 (339)	1.24	91% HOMO-1 → LUMO	π–π* (1)	3.96 (313)
	4	4.13 (300)	0.24	70% HOMO → LUMO + 3	π–π* (2)	
	5	4.14 (300)	0.13	62% HOMO → LUMO + 2	π–π* (3)	
p1B	1	2.87 (432)	0.97	97% HOMO → LUMO	CT	3.17 (322)
	3	3.93 (316)	0.67	75% HOMO-1 → LUMO	π–π* (1)	4.16 (298)
	4	4.00 (310)	0.18	87% HOMO → LUMO + 3	π–π* (2)	
m2B	1	3.26 (381)	0.03	97% HOMO → LUMO	CT	3.58 (346)
	2	4.05 (306)	0.18	96% HOMO → LUMO + 1	π–π* (1)	4.16 (298)
	3	4.17 (298)	0.23	94% HOMO → LUMO + 2	π–π* (2)	
p2B	1	3.67 (338)	0.46	96% HOMO → LUMO	CT	3.77 (329)
	3	4.16 (298)	0.18	88% HOMO → LUMO + 2	π–π* (1)	4.03 (308)

[a] Order of calculated transitions according to energy.

Fig. 4. For *meta*-conjugated dyes, the electron density in the HOMO is confined around the TPA donors, while that of the LUMO on the cyanoacrylic acid or benzoic acid acceptors. The electron distribution in the HOMO of *para*-conjugated dyes delocalized more extended than that of the *meta*-conjugated isomers. The electron distribution in the LUMO of cyanoacrylic acid group is more localized than that of the benzoic acid group, and the potential energy level of the former is lower than that of the latter owing to a greater electron-withdrawing ability (Table 3). Electron movement from the donor to the acceptor is most efficient for the chromophores possessing a *para*-linked donor and a cyanoacrylic acid acceptor, i.e., compounds in the **pA** series, upon the irradiation of light.

The TDDFT excited states calculations were performed on the lowest 10 singlet-singlet excitations of dyes **A** and **B**, neglecting the influence of solvent. The results of transitions with oscillator strength above 0.1 are summarized in Table 3, except the lowest transition for *meta* derivatives in order for comparisons. The lowest transitions correspond mainly to ICT transitions as reflected by the electron distributions, and can also be verified by the large dipole moments displayed in Table 2. The estimated oscillator strengths of *meta* derivatives are significantly smaller than the corresponding ones of *para* isomers, e.g., the $S_0 \rightarrow S_1$ transition of **m1A** vs **p1A**, suggesting that the value of f is associated closely with the π-conjugation interaction. These calculated f values in Table 3 are in excellent agreement with the experimental parameters listed in Table 1. The most prominent long wavelength absorptions for the *meta*-substituted compounds are the HOMO-1 → LUMO transitions. It involves an electron migration from the stilbene (π) chromophore, instead of the TPA chromophore, toward the acceptor (π^*). This assignment can be verified by comparing the absorption spectrum of *meta*-isomer with that of 2-cyano-3-(p-styrylphenyl)acrylic acid (Figure S4) without a TPA moiety. The lower degree of resonance between stilbene and the *meta*-linked TPA interrupted the direct electronic coupling between TPA and the acceptor group. The computed results comply remarkably well with the observed spectral characteristics of *meta*-isomers as shown in Fig. 1. The substantially low absorptivity of the long wavelength HOMO → LUMO transition in *meta*-substituted derivatives, nevertheless, is responsible for their low quantum efficiency of DSSCs.

3.5. Electrochemical properties

The redox potentials of all compounds were measured to ensure the feasibility of electron transfer from the dyes to the TiO_2 conductive band. The cyclic voltammetry (CV) was done in THF solution containing 0.1 M tetrabutylammonium hexafluorophosphate ($TBAPF_6$) as the supporting electrolyte, $Ag/AgNO_3$ as the reference electrode, and a standard ferrocene/ferrocenium redox system as an internal standard. The potential level of highest occupied molecular orbital (HOMO) was estimated from the first oxidative wave (E_{ox}) as listed in Table 4. Evidently, the HOMO levels of all dyes are more positive than the reducing potential of iodine/iodide (0.4 V versus NHE) pair, therefore there is sufficient driving force for the oxidized dyes to recapture an electron from the electrolyte. The oxidation potentials of *meta* dyes are found to be close to the corresponding *para* isomers (e.g., **m1A/p1A** and **m2A/p2A**), indicating the similarity in the electron-donating ability of *meta* and *para* derivatives (c.f. Table 3). The lowest unoccupied molecular orbital (LUMO) levels of the dyes were estimated from the first oxidation potential and the 0-0 transition value ($E_{0\text{-}0}$) measured from the intersection of normalized absorption and fluorescence spectra. The LUMO levels are higher than the TiO_2 conductive band (−0.5 V), and thus warrants a sufficient driving force for electrons injecting into conductive band. A comparison between dyes **A** and **B** indicates that the latter displayed a higher reductive potential level as well as a wider HOMO → LUMO transition band gap.

3.6. Photovoltaic performance of DSSCs

The solar cells were fabricated by using these dyes as sensitizers coated on the surface of TiO_2 electrodes, and the parameters were measured under simulated AM 1.5G irradiation (100 mW cm^{-2}). A typical DSSCs device has an effective area of 0.25 cm^2 and an electrolyte composed of I_2 (0.05 M), LiI (0.5 M), and *tert*-butylpyridine (0.5 M) in acetonitrile solution. The open-circuit photovoltage (V_{oc}), short-circuit photocurrent density (J_{sc}), fill factor (ff), and solar-to-electrical energy conversion efficiencies (η) are summarized in Table 4, where N719 is included as a comparison. Although all the devices were fabricated under the same condition, the quantity of dyes which has been absorbed by TiO_2 depends on the nature of the materials. Our analyses indicated that the loading amount of *para* isomers was a little higher than that of the *meta* isomers (Table T1), that may be ascribed to the more symmetrical geometry of the former.

The *I–V* curves of all dyes are shown in Fig. 5. For dyes of type **A**, the introduction of cyanoacrylic acid as the electron acceptor contributed to a bathochromic shift of both the absorption and emission spectra with respect to the corresponding type **B** dyes. The more extended conjugation length in dye group **A** leads to higher J_{sc}, V_{oc}, and ff values, and consequently to a higher energy conversion efficiencies than those in dye group **B**. For the dye with the same acceptor group (either series **A** or **B**), the J_{sc} and V_{oc} values of the *para* derivatives are larger than the corresponding *meta* ones.

The incident photo-to-current conversion efficiencies (IPCE) spectra of dyes **A** and **B** were shown in Fig. 6, and the IPCE spectra of all the dyes are red-shifted comparing to the absorption spectra in solutions, which could be attributed to the interaction between the dyes and the TiO_2 nanostructure [29]. In general, compounds with a cyanoacrylate anchoring group (group **A**) show broader IPCE spectra and higher IPCE values than those with a benzoate (group **B**).

The change of a *para*-substituent to a *meta* position brings about a difference in the electronic configurations [40]. It is well-known that a *meta*-connected molecule induces a smaller electronic coupling in the ground state (μ_g) between the donor and the acceptor. The μ_e values of *meta* isomers in dyes **A** and **B** are close to those of the *para* isomers (Table 2), indicating a similar charge separated state is formed in the excited state. The ability of electron injection from *meta*-isomers to TiO_2 conductive band is expected to be as effective as from the *para*-isomers. The ICT transitions in both isomers can be clearly depicted by quantum mechanical calculations. It shows that the *meta*-isomers exhibit a substantially weaker HOMO → LUMO transition with respect to the *para* isomers. The major absorption band of *meta*-isomers appears on the HOMO-1 → LUMO transition, which exhibits an apparent blue-shift of ca. 50–100 nm with respect to the *para*-isomers (Fig. 2 and Table 3). Therefore the *meta*-isomers display narrower IPCE spectra in comparison with the corresponding *para*-isomers, along with smaller J_{sc} values (Table 4).

Nevertheless it is important to note that, despite the narrower absorption band width, the *meta*-isomers **m1A** and **m1B** did exhibit higher IPCE value within their maximal absorption range in a short-wavelength region. For example, it is clearly observed in Fig. 6(a) that in the wavelength region of <400 nm, compound **m1A** displayed the highest IPCE value. This phenomenon may be even more pronounced while considering the lower loading amount of the *meta*-isomers in the fabrication of devices. It is consistent with the earlier observations that the *meta*-isomers tend to be more stabilized in the ICT state. They display a longer fluorescent lifetime,

Table 4
Electrochemical properties and photovoltaic performance of DSSCs.

Dye	E_{ox} (V[a])	E_{0-0} (eV[b])	E_{red} (V[c])	V_{oc} (mV)	J_{sc} (mA cm^{-2})	ff	η (%)
N719	0.70[d]	2.40 [d]	−1.70[d]	0.72	15.15	0.60	6.50
m1A	1.20	2.73	−1.53	0.62	5.47	0.66	2.23
p1A	1.15	2.57	−1.42	0.64	10.44	0.62	4.12
m2A	1.32	2.71	−1.39	0.65	2.98	0.66	1.27
p2A	1.26	2.65	−1.39	0.66	6.94	0.64	2.92
m1B	1.21	3.02	−1.81	0.58	1.47	0.57	0.48
p1B	1.18	2.92	−1.74	0.62	4.62	0.62	1.78
m2B	1.30	3.17	−1.87	0.44	0.39	0.47	0.08
p2B	1.36	3.32	−1.96	0.60	2.31	0.60	0.83

[a] Oxidation potential in THF vs NHE.
[b] Measured at the intersection of absorption and emission spectra.
[c] Calculated from E_{ox} and E_{0-0}.
[d] Data from Ref. [57].

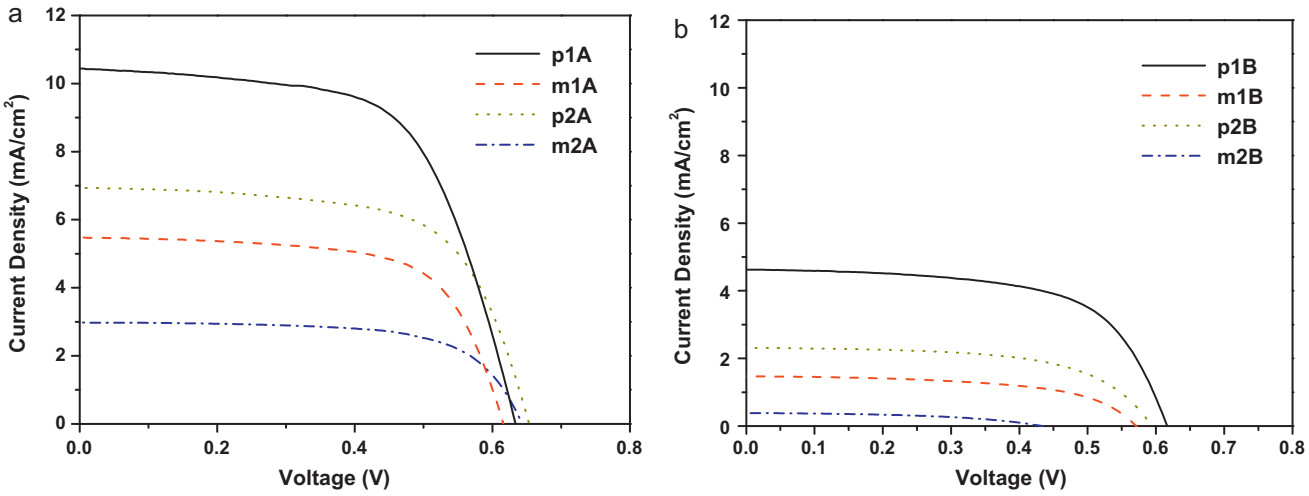

Fig. 5. Current-voltage characteristics of the DSSCs based on (a) dyes **A** and (b) dyes **B**.

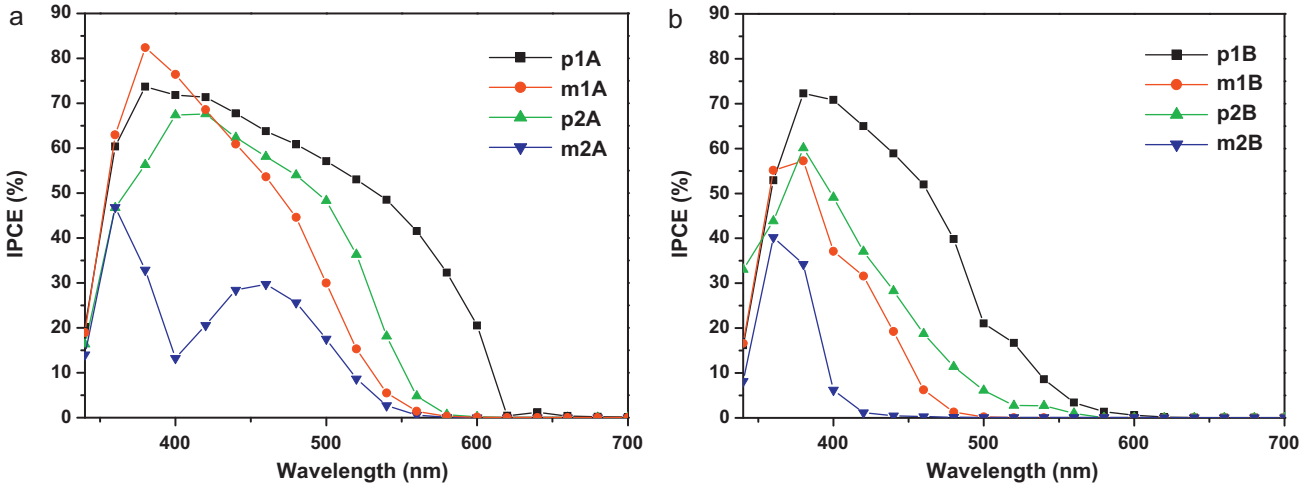

Fig. 6. IPCE spectra of DSSCs based on (a) dyes **A** and (b) dyes **B**.

which indicate a slower rate of internal charge recombination and a higher injection efficiency to the TiO_2 conducting band.

4. Conclusions

According to the solvent dependence of the fluorescence spectra of dyes **A** and **B**, it is without doubt that both the *meta* and *para*-isomers were able to induce a significant charge separation upon photo-excitation. The major absorption band of *para*-isomers is derived from a HOMO → LUMO transition, yet for *meta*-isomers it comes from a higher energy HOMO-1 → LUMO transition. This phenomenon correlates well with the TDDFT calculations. The *meta* linkage dyes therefore show a narrower and weaker absorption band in comparison with the *para* isomers. As a result, the *meta*-substituted dyes yielded a narrower IPCE spectrum, a lower J_{sc} value, and consequently a smaller η value. However, it is imperative to note that at certain short wavelength region where the

meta-isomers exhibited high degree of absorption, the IPCE value of *meta*-isomers become higher than that of *para*-isomers.

Acknowledgments

Financial supports were provided by the Institute of Chemistry, Academia Sinica, and the National Science Council of the Republic of China. We thank Professor J.-S. Yang (NTU) for his assistance on measuring the lifetimes.

Appendix A. Supplementary data

Supplementary data associated with this article can be found, in the online version, at doi:10.1016/j.jphotochem.2011.05.022.

References

[1] B. O'Regan, M. Grätzel, A low-cost, high-efficiency solar cell based on dye-sensitized colloidal TiO_2 films, Nature 353 (1991) 737–740.
[2] M Grätzel, Conversion of sunlight to electric power by nanocrystalline dye-sensitized solar cells, J. Photochem. Photobiol. A 164 (2004) 3–14.
[3] M.K. Nazeeruddin, A. Kay, L. Rodicio, R. Humphry-Baker, E. Müller, P. Liska, N. Vlachopoulos, M. Grätzel, Conversion of light to electricity by *cis*-X_2Bis(2,2′-bipyridyl-4,4′-dicarboxylate)ruthenium(II) charge-transfer sensitizers (X = C1$^-$, Br$^-$ I$^-$, CN$^-$, and SCN$^-$) on nanocrystalline TiO_2 electrodes, J. Am. Chem. Soc. 115 (1993) 6382–6390.
[4] M.K. Nazeeruddin, P. Péchy, T. Renouard, S.M. Zakeeruddin, R. Humphry-Baker, P. Comte, P. Liska, L. Cevey, E. Costa, V. Shklover, L. Spiccia, G.B. Deacon, C.A. Bignozzi, M. Grätzel, Engineering of efficient panchromatic sensitizers for nanocrystalline TiO_2-based solar cells, J. Am. Chem. Soc. 123 (2001) 1613–1624.
[5] Z. Wang, Y. Cui, K. Hara, Y. Dan-oh, C. Kasada, A. Shinpo, A high-light-harvesting-efficiency coumarin dye for stable dye-sensitized solar cells, Adv. Mater. 19 (2007) 1138–1141.
[6] Z. Wang, Y. Cui, Y. Dan-oh, C. Kasada, A. Shinpo, K. Hara, Thiophene-functionalized coumarin dye for efficient dye-sensitized solar cells: electron lifetime improved by coadsorption of deoxycholic acid, J. Phys. Chem. C 111 (2007) 7224–7230.
[7] K. Hara, Y. Abe, M. Yanagida, Electron transport in coumarin-dye-sensitized nanocrystalline TiO_2 electrodes, J. Phys. Chem. B 109 (2005) 23776–23778.
[8] K. Sayama, K. Hara, N. Mori, M. Satsuki, S. Suga, S. Tsukagoshi, Y. Abe, H. Sugihara, H. Arakawa, Photosensitization of a porous TiO_2 electrode with merocyanine dyes containing a carboxyl group and a long alkyl chain, Chem. Commun. (2000) 1173–1174.
[9] K. Sayama, S. Tsukagoshi, K. Hara, Y. Ohga, A.K. Shinpou, Y. Abe, S. Suga, H. Arakawa, Photoelectrochemical properties of J aggregates of benzothiazole merocyanine dyes on a nanostructured TiO_2 film, J. Phys. Chem. B 106 (2002) 1363–1371.
[10] A. Ehret, L. Stuhl, M.T. Spitler, Spectral sensitization of TiO_2 nanocrystalline electrodes with aggregated cyanine dyes, J. Phys. Chem. B 105 (2001) 9960–9965.
[11] K. Sayama, K. Hara, Y. Ohga, A. Shinpou, S. Suga, H. Arakawa, Significant effects of the distance between the cyanine dye skeleton and the semiconductor surface on the photoelectrochemical properties of dye-sensitized porous semiconductor electrodes, New J. Chem. 25 (2001) 200–202.
[12] D. Kuang, S. Uchida, R. Humphry-Baker, S.M. Zakeeruddin, M. Grätzel, Organic dye-sensitized ionic liquid based solar cells: remarkable enhancement in performance through molecular design of indoline sensitizers, Angew. Chem. Int. Ed. 47 (2008) 1923–1927.
[13] Y.J. Chang, T.J. Chow, Dye-sensitized solar cell utilizing organic dyads containing triarylene conjugates, Tetrahedron 65 (2009) 4726–4734.
[14] Y.J. Chang, T.J. Chow, Triaryl linked donor acceptor dyads for high-performance dye-sensitized solar cells, Tetrahedron 65 (2009) 9626–9632.
[15] J. Song, F. Zhang, C. Li, W. Liu, B. Li, Y. Huang, Z. Bo, Phenylethyne-bridged dyes for dye-sensitized solar cells, J. Phys. Chem. C 113 (2009) 13391–13397.
[16] S. Qu, W. Wu, J. Hua, C. Kong, Y. Long, H. Tian, New diketopyrrolopyrrole (DPP) dyes for efficient dye-sensitized solar cells, J. Phys. Chem. C 114 (2010) 1343–1349.
[17] W. Xu, B. Peng, J. Chen, M. Liang, F. Cai, J. Phys. Chem. C 112 (2008) 874–880.
[18] S.-T. Huang, Y.-C. Hsu, Y.-S. Yen, H.H. Chou, J.T. Lin, C.-W. Chang, C.-P. Hsu, C. Tsai, D.-J. Yin, New triphenylamine-based dyes for dye-sensitized solar cells, J. Phys. Chem. C 112 (2008) 19739–19747.
[19] H. Tian, X. Yang, R. Chen, R. Zhang, A. Hagfeldt, L. Sun, Effect of different dye baths and dye-structures on the performance of dye-sensitized solar cells based on triphenylamine dyes, J. Phys. Chem. C 112 (2008) 11023–11033.
[20] G. Zhang, H. Bala, Y. Cheng, D. Shi, X. Lv, Q. Yu, P. Wang, High efficiency and stable dye-sensitized solar cells with an organic chromophore featuring a binary π-conjugated spacer, Chem. Commun. (2009) 2198–2200.
[21] G. Li, K.-J. Jiang, Y.-F. Li, S.-L. Li, L.-M. Yang, Efficient structural modification of triphenylamine-based organic dyes for dye-sensitized solar cells, J. Phys. Chem. C 112 (2008) 11591–11599.
[22] S. Hwang, J.H. Lee, C. Park, H. Lee, C. Kim, C. Park, M.-H. Lee, W. Lee, J. Park, K. Kim, N.-G. Park, C. Kim, A highly efficient organic sensitizer for dye-sensitized solar cells, Chem. Commun. (2007) 4887–4889.
[23] H. Tian, X. Yang, J. Cong, R. Chen, J. Liu, Y. Hao, A. Hagfeldt, L. Sun, Tuning of phenoxazine chromophores for efficient organic dye-sensitized solar cells, Chem. Commun. (2009) 6288–6290.
[24] Z. Ning, X. Tian, Triarylamine: a promising core unit for efficient photovoltaic materials, Chem. Commun. (2009) 5483–5495.
[25] H.-Y. Yang, Y.-S. Yen, Y.-C. Hsu, H.-H. Chou, J.T. Lin, Organic Dyes Incorporating dithieno[3 2-b:2′,3′-d]thiophene moiety for efficient dye-sensitized solar cells, Org. Lett. 12 (2010) 16–19.
[26] C. Teng, X. Yang, C. Yuan, C. Li, R. Chen, H. Tian, S. Li, A. Hagfeldt, L. Sun, Two novel carbazole dyes for dye-sensitized solar cells with open-circuit voltages up to 1 V based on Br^-/Br_3, Org. Lett. 11 (2009) 5542–5545.
[27] X.-H. Zhang, Z.-S. Wang, Y. Cui, N. Koumura, A. Furube, K. Hara, Organic sensitizers based on hexylthiophene-functionalized indolo[3 2-b]carbazole for efficient dye-sensitized solar cells, J. Phys. Chem. C 113 (2009) 13409–13415.
[28] K.R.J. Thomas, J.T. Lin, Y.-C. Hsu, K.-C. Ho, Organic dyes containing thienylfluorene conjugation for solar cells, Chem. Commun. (2005) 4098–4100.
[29] D. Heredia, J. Natera, M. Gervaldo, L. Otero, F. Fungo, C.-Y. Lin, K.-T. Wong, Spirobifluorene-bridged donor/acceptor dye for organic dye-sensitized solar cells, Org. Lett. 12 (2010) 12–15.
[30] J.-S. Yang, Y.-D. Lin, Y.-H. Lin, F.-L. Liao, Zn(II)-induced ground-state π-deconjugation and excited-state electron transfer in *N*,*N*-bis(2-pyridyl)amino-substituted arenes, J. Org. Chem. 69 (2004) 3517–3525.
[31] J.-S. Yang, Y.-D. Lin, Y.-H. Chang, S.S. Wang, Synthesis, dual fluorescence, and fluoroionophoric behavior of dipyridylaminomethylstilbenes, J Org. Chem. 70 (2005) 6066–6073.
[32] C.-W. Lee, H.-P. Lu, C.-M. Lan, Y.-L. Huang, Y.-R. Liang, W.-N. Yen, Y.-C. Liu, Y.-S. Lin, E.W.-G. Diau, C. -Y, Novel zinc porphyrin sensitizers for dye-sensitized solar cells: synthesis and spectral, electrochemical, and photovoltaic properties, Chem Eur. J. 15 (2009) 1403–1412.
[33] P.Y. Reddy, L. Giribabu, C. Lyness, H.J. Snaith, C. Vijaykumar, M. Chandrasekharam, M. Lakshmikantam, J.-H. Yum, K. Kalyanasundaram, M. Grätzel, M.K. Nazeeruddin, Efficient sensitization of nanocrystalline TiO_2 films by a near-IR absorbing unsymmetrical zinc phthalocyanine, Angew. Chem. Int. Ed. 46 (2007) 373–376.
[34] K.-F. Chen, Y.-C. Hsu, Q. Wu, M.-C.-P. Yeh, S.-S. Sun, Structurally simple dipolar organic dyes featuring 1 3-cyclohexadiene conjugated unit for dye-sensitized solar cells, Org. Lett. 11 (2009) 377–380.
[35] K.M. Gaab, A.L. Thompson, J. Xu, T.J. Martinez, C.J. Bardeen, Meta-conjugation and excited-state coupling in phenylacetylene dendrimers, J. Am. Chem. Soc. 125 (2003) 9288–9289.
[36] A.L. Thompson, T.-S. Ahn, K.R.J. Thomas, S. Thayumanavan, T.J. Martinez, C.J. Bardeen, Using meta conjugation to enhance charge separation versus charge recombination in phenylacetylene donor-bridge-acceptor complexes, J. Am. Chem. Soc. 127 (2005) 16348–16349.
[37] J.-S. Yang, K.-L. Liau, C.-Y. Li, M.-Y. Chen, Meta conjugation effect on the torsional motion of aminostilbenes in the photoinduced intramolecular charge-transfer state, J. Am. Chem. Soc. 129 (2007) 13183–13192.
[38] J.-S. Yang, K.-L. Liau, C.-W. Tu, C.-Y. Hwang, Excited-state behavior of *N*-phenyl-substituted trans-3-aminostilbenes: where the"*m*-amino effect" meets the "amino-conjugation effect", J. Phys. Chem. A 109 (2005) 6450–6456.
[39] F.D. Lewis, J.-S. Yang, The excited state behavior of aminostilbenes. a new example of the meta effect, J. Am. Chem. Soc. 119 (1997) 3834–3835.
[40] F.D. Lewis, R.S. Kalgutkar, J.-S. Yang, The photochemistry of *trans-ortho*-, *-meta*-, and *-para*-aminostilbenes, J Am. Chem. Soc. 121 (1999) 12045–12053.
[41] F.D. Lewis, W. Weigel, Excited state properties of donor-acceptor substituted *trans*-stilbenes: the *meta*-amino effect, J. Phys. Chem. A 104 (2000) 8146–8153.
[42] F.D. Lewis, W. Weigel, X. Zuo, Relaxation pathways of photoexcited diaminostilbenes. the *meta*-amino effect, J. Phys. Chem. A 105 (2001) 4691–4696.
[43] M.M. Oliva, J. Casado, G. Hennrich, J.T.L. Navarrete, Octopolar chromophores based on donor- and acceptor-substituted 1 3,5-tris(phenylethynyl)benzenes: impact of meta-conjugation on the molecular and electronic structure by means of spectroscopy and theory, J. Phys. Chem. B 106 (2006) 19198–19206.
[44] J.-S. Yang, Y.-R. Lee, J.-L. Yan, M.-C. Lu, Synthesis and properties of a fluorene-capped isotruxene: a new unsymmetrical star-shaped π-System, Org. Lett. 8 (2006) 5813–5816.
[45] Q. Chu, Y. Pang, L. Ding, F.E. Karasz, Synthesis, chain rigidity, and luminescent properties of poly[(1,3-phenyleneethynylene)-*alt*-tris(2,5-dialkoxy-1,4-phenyleneethynylene)]s, Macromolecules 35 (2002) 7569–7574.
[46] H. Gilman, G.E. Brown, Anomalous metalation of triphenylamine, J. Am. Chem. Soc. 62 (1940) 3208–3210.
[47] A.S.-Y. Lee, C.-L. Cheng, A novel and selective method for hydrolysis of acetals and ketals, Tetrahedron 53 (1997) 14255–14262.
[48] W. Masato, Y. Toshihide, N. Shoichi, K. Yasuyuki, Preparation of formyltriarylamines, Tosoh Corp (JP), Patent 2000007627 (2000).
[49] L. Deng, P.T. Furuta, S. Garon, J. Li, D. Kavulak, M.E. Thompson, J.M.J. Fréchet, Living radical polymerization of bipolar transport materials for highly efficient light emitting diodes, Chem. Mater 18 (2006) 386–395.
[50] E. Grimley, D.H. Collum, E.G. Alley, B. Layton, ^{13}C NMR study of ortho-, meta-, and para-substituted phenyldiphenylamines: substituent effect correlations, Org. Magn. Reson. 15 (1981) 296–302.
[51] M.J. Frisch, G.W. Trucks, H.B. Schlegel, G.E. Scuseria, M.A. Robb, J.R. Cheeseman, J.A. Montgomery Jr., T. Vreven, K.N. Kudin, J.C. Burant, J.M. Millam, S.S. Iyengar, J. Tomasi, V. Barone, B. Mennucci, M. Cossi, G. Scalmani, N. Rega, G.A.

Petersson, H. Nakatsuji, M. Hada, M. Ehara, K. Toyota, R. Fukuda, J. Hasegawa, M. Ishida, T. Nakajima, Y. Honda, O. Kitao, H. Nakai, M. Klene, X. Li, J.E Knox, H.P. Hratchian, J.B. Cross, V. Bakken, C. Adamo, J. Jaramillo, R. Gomperts, R.E. Stratmann, O. Yazyev, A.J. Austin, R. Cammi, C. Pomelli, J.W. Ochterski, P.Y. Ayala, K. Morokuma, G.A. Voth, P. Salvador, J.J. Dannenberg, V.G. Zakrzewski, S. Dapprich, A.D. Daniels, M.C. Strain, O. Farkas, D.K. Malick, A.D. Rabuck, K. Raghavachari, J.B. Foresman, J.V. Ortiz, Q. Cui, A.G. Baboul, S. Clifford, J. Cioslowski, B.B. Stefanov, G. Liu, A. Liashenko, P. Piskorz, I. Komaromi, R.L. Martin, D.J. Fox, T. Keith, M.A. Al-Laham, C.Y. Peng, A. Nanayakkara, M. Challacombe, P.M.W. Gill, B. Johnson, W. Chen, M.W. Wong, C. Gonzalez, J.A. Pople, Gaussian 03, Gaussian Inc., Pittsburgh, PA, 2003.

[52] A.D. Becke, Density-functional thermochemistry. III. The role of exact exchange, J. Chem. Phys. 98 (1993) 5648–5652.

[53] R. Ditchfield, W.J. Hehre, J.A. Pople, Self-consistent molecular-orbital methods. IX. an extended gaussian-type basis for molecular-orbital studies of organic molecules, J. Chem. Phys. 54 (1971) 724–728.

[54] H.K. Sinha, K. Yates, Effects of positions of donor and acceptor type substituents on ground- and excited-state charge transfer: electrochromism of some benzene derivatives, J. Am. Chem. Soc. 113 (1991) 6062–6067.

[55] W. Baumann, H. Bischof, J.-C. Fröhling, C. Brittinger, W. Rettig, K. Rotkiewicz, Considerations on the dipole moment of molecules forming the twisted intramolecular charge transfer state, J. Photochem. Photobiol. A 64 (1992) 49–72.

[56] A. Hagfeldt, M. Grätzel, Molecular photovoltaics, Acc. Chem. Res. 33 (2000) 269–277.

[57] M.K. Nazeeruddin, F.D. Angelis, S. Fantacci, A. Selloni, G. Viscardi, P. Liska, S. Ito, B. Takeru, M. Grätzel, Combined experimental and DFT-TDDFT computational study of photoelectrochemical cell ruthenium sensitizers, J. Am. Chem. Soc. 127 (2005) 16835–16847.